The global budgets of organic hydroperoxides for present and pre-industrial scenarios

ARTICLE *in* ATMOSPHERIC ENVIRONMENT · JUNE 2015

Impact Factor: 3.28 · DOI: 10.1016/j.atmosenv.2015.03.045

10 AUTHORS, INCLUDING:

Anwar H Khan

University of Bristol

29 PUBLICATIONS **135** CITATIONS

SEE PROFILE

S. R. Utembe

University of Melbourne

38 PUBLICATIONS **705** CITATIONS

SEE PROFILE

Alexander Thomas Archibald

University of Cambridge

45 PUBLICATIONS **404** CITATIONS

SEE PROFILE

Dudley E. Shallcross

University of Bristol

239 PUBLICATIONS **3,498** CITATIONS

SEE PROFILE

Atmospheric Environment 110 (2015) 65–74

Contents lists available at ScienceDirect

Atmospheric Environment

journal homepage: www.elsevier.com/locate/atmosenv

The global budgets of organic hydroperoxides for present and pre-industrial scenarios

M.A.H. Khan [a], M.C. Cooke [a, 1], S.R. Utembe [a, 2], P. Xiao [a], W.C. Morris [a], R.G. Derwent [b], A.T. Archibald [a, 3], M.E. Jenkin [a, c], C.J. Percival [d], D.E. Shallcross [a, *]

[a] Biogeochemistry Research Centre, School of Chemistry, University of Bristol, Cantock's Close, Bristol BS8 1TS, UK
[b] rdscientific, Newbury, Berkshire, UK
[c] Atmospheric Chemistry Services, Okehampton, Devon EX20 4QB, UK
[d] The Centre for Atmospheric Science, The School of Earth, Atmospheric and Environmental Science, The University of Manchester, Simon Building, Brunswick Street, Manchester M13 9PL, UK

HIGHLIGHTS

- The formation of ROOH from RO_2 and HO_2 is significant under NO_x-limited conditions.
- The global burden of ROOH is found to be 3.8 Tg.
- ROOH peak near the equator having higher photochemistry and large VOC emissions.
- HO_x recycling caused significant increases in ROOH over tropical forested regions.

ARTICLE INFO

Article history:
Received 18 September 2014
Received in revised form
30 January 2015
Accepted 22 March 2015
Available online 24 March 2015

Keywords:
Organic hydroperoxides
STOCHEM-CRI model
HO_x recycling mechanism
Present day simulation
Pre-industrial scenario

ABSTRACT

The global 3-D chemistry-transport model, STOCHEM-CRI (Utembe et al., 2010), has been used to simulate the global distribution of organic hydroperoxides (ROOH) for both present day and pre-industrial scenarios. Globally, the formation of ROOH is solely from the reaction between RO_2 and HO_2, being more significant under NO_x-limited conditions; here the self and cross reactions of RO_2 and HO_2 radicals dominate over their reaction with NO. The predominant global loss processes for ROOH are reaction with OH (95%) and by photolysis (4.4%) with a minor loss (<1%) by deposition, in the present day scenario. The associated global burden of ROOH in our model study is found to be 3.8 Tg. The surface distribution of ROOH shows a peak near the equator corresponding with higher photochemical activity and large (biogenic) VOC emissions. The simulated abundances of ROOH are comparable with those recorded in field campaigns, but generally show a tendency towards underestimation, particularly in the boundary layer. ROOH displayed seasonal cycles with higher concentrations during the summer months and lower concentrations during the winter months. The effects of including proposed HO_x recycling schemes, including isomerisation of isoprene-derived peroxy radicals on the global budget of ROOH have also been investigated for the present and the pre-industrial environment. The present day simulations showed significant increases in CH_3OOH and ROOH (up to 80% and 30%, respectively) over tropical forested regions, due to a general increase in HO_2 and RO_2 levels in isoprene-rich regions at low NO_x levels. In the pre-industrial scenario, the increases in CH_3OOH and total ROOH abundances are even larger, reflecting the more efficient operation of HO_x recycling mechanisms at lower NO_x levels. RCO_3H species contribute 40–50% of the global burden of ROOH; inclusion of HO_x recycling mechanisms leads to an increase in these RCO_3H species but there is no discernible change in the remaining ROOH (ROOH–RCO_3H) burden.

1. Introduction

Organic hydroperoxides (ROOH) play a significant role in atmospheric processes such as acting as important temporary reservoirs for tropospheric HO_x and RO_x radicals (Madronich and

* Corresponding author.
E-mail address: d.e.shallcross@bristol.ac.uk (D.E. Shallcross).
[1] Now at the Met Office, FitzRoy Road, Exeter, Devon EX1 3PB, UK.
[2] Now at the School of Earth Sciences, University of Melbourne, Parkville, VIC 3010, Australia.
[3] Now at the NCAS-Climate and the Centre for Atmospheric Science, University of Cambridge, Cambridge, UK.

http://dx.doi.org/10.1016/j.atmosenv.2015.03.045

Calvert, 1990; Lightfoot et al., 1992) and in the formation of secondary organic aerosols (He et al., 2010; Utembe et al., 2011; Lin et al., 2012). They are strong oxidants like ozone, and have some toxic effects on plants by inactivation of enzymes, impairing metabolic processes, and blanching chlorophyll (Hewitt et al., 1990; Hewitt and Terry, 1992; Polle and Junkermann, 1994). Methyl hydroperoxide (CH_3OOH), the most abundant organic hydroperoxide, has a longer lifetime of 2–3 days and is less soluble in water than hydrogen peroxide (H_2O_2) (Cohan et al., 1999; Mari et al., 2000; Wang and Chen, 2006). CH_3OOH can thus be transported into the upper troposphere by deep convection, consequently leading to the redistribution of HO_x and RO_x radicals in different altitudes and different regions (Jaeglé et al., 1997; Cohan et al., 1999; Mari et al., 2000; Ravetta et al., 2001). Aircraft observations in the upper troposphere have shown evidence for enhanced HO_x in convective outflow (Brune et al., 1998) as well as for enhanced CH_3OOH (Cohan et al., 1999).

Biomass burning has been found to be an important source of ROOH (Snow et al., 2007; Lee and Heikes, 1997). No other significant direct emissions of ROOH from natural or anthropogenic sources have been reported to date. It is believed that the main mechanism of formation is by the reaction of hydroperoxy radicals (HO_2) with organic peroxy radicals (RO_2), which are produced through the photochemical reactions of volatile organic compounds (VOCs) (Gunz and Hoffmann, 1990; Madronich and Calvert, 1990; Sakugawa et al., 1990; Lightfoot et al., 1992).

$$RO_2 + HO_2 \rightarrow ROOH + O_2 \quad \text{(R1)}$$

The production of ROOH is affected by the levels of trace gases (such as NO_x, VOC, CO, and O_3) and by meteorological parameters (such as light intensity, temperature, water vapour concentration, and pressure) (Kleinman, 1986, 1991; Logan et al., 1981). At higher O_3 and CO levels, the formation of HO_2 increases following reactions (R2) to (R4).

$$O_3 + h\nu\ (\lambda \leq 320\ \text{nm}) \rightarrow O\ (^1D) + O_2 \quad \text{(R2)}$$

$$O\ (^1D) + H_2O \rightarrow 2OH \quad \text{(R3)}$$

$$HO + CO\ (+O_2) \rightarrow HO_2 + CO_2 \quad \text{(R4)}$$

The concentration of RO_2 increases with increasing levels of VOCs followed by their oxidation initiated by reaction with OH radicals, which is important for all VOCs, and with NO_3 radicals for alkenes.

$$VOC + OH\ (+O_2) \rightarrow RO_2 \quad \text{(R5)}$$

$$Alkene + NO_3\ (+O_2) \rightarrow RO_2 \quad \text{(R6)}$$

At higher levels of NO_x, the ROOH formation is substantially suppressed by the reaction of NO with HO_2 and RO_2.

$$RO_2 + NO \rightarrow RO + NO_2 \quad \text{(R7)}$$

$$HO_2 + NO \rightarrow OH + NO_2 \quad \text{(R8)}$$

However, lower levels of NO_x favour the formation of ROOH, leading to a general suppression of the abundance of free radical species. The major sinks for ROOH are the reactions with OH radicals, photolysis, dry deposition, and wet deposition (Kleinman, 1986; Sakugawa et al., 1990).

Production of ROOH has also been observed from the ozonolysis of alkenes under humid conditions (Hua et al., 2008). Laboratory studies of the gas-phase ozonolysis of alkenes (e.g. ethene, isoprene, α-pinene) have shown that the contribution of the ozonolysis reaction to the production of ROOH is significant (Simonaitis et al., 1991; Hewitt and Kok, 1991; Horie et al., 1994; Chen et al., 2008; Zhang et al., 2009),

$$Alkene + O_3 \rightarrow \alpha CI + (1-\alpha)\ SCI + carbonyl \quad \text{(R9)}$$

$$SCI + H_2O \rightarrow ROOH \quad \text{(R10)}$$

where, CI denotes an “excited” Criegee intermediate, and SCI a “stabilised” Criegee intermediate.

Over the past two decades, significant levels of CH_3OOH as well as higher alkyl ROOH have been observed in the atmosphere (Heikes, 1992; Heikes et al., 1996; Jackson and Hewitt, 1996; Ayers et al., 1996; Lee et al., 1998; Weinstein-Lloyd et al., 1998; O'Sullivan et al., 1999; Morgan and Jackson, 2002; Takami et al., 2003; Grossmann et al., 2003; Valverde-Canossa et al., 2005; Hua et al., 2008; Frey et al., 2005, 2009; Ren et al., 2009; He et al., 2010; Zhang et al., 2012). However, overall the number of long-term measurements of atmospheric ROOH is small where most consist of short-term records at or near the surface area. Hence, the observed ROOH concentrations and their interpretation in terms of budgets is less well understood than other oxygenated species such as methanol and acetone. The transport of ROOH can also have important regional and global effects on radical concentration (Jaeglé et al., 1997). So the knowledge and understanding of the distribution and global budget of ROOH are necessary to assess their potential ability to affect the atmospheric oxidation potential and in their role as a potential marker of the oxidation production efficiency. In this study, the global distribution of 42 organic hydroperoxides (ROOH) is presented using the STOCHEM-CRI global 3-dimensional chemistry transport model (Utembe et al., 2010). The seasonal cycle and the global budget of ROOH have been determined for the present and pre-industrial scenarios. Archibald et al. (2010) have previously implemented additional HO_x recycling mechanisms involving isomerisation of isoprene-derived peroxy radicals (Peeters et al., 2009) and propagating channels for the reactions of HO_2 with acyl peroxy radicals (e.g. Hasson et al., 2012) into STOCHEM-CRI. The effects of including these additional HO_x recycling mechanisms are also illustrated and discussed.

2. Experimental

2.1. Global chemistry transport model STOCHEM-CRI

A global 3-dimensional Chemistry Transport Model, STOCHEM used in this study, is a Lagrangian approach, where the troposphere is divided into 50,000 air parcels, which are advected every 3 h by wind from the Meteorological Office Hadley Centre general circulation model (GCM). The Lagrangian cells are based on a grid of 1.25° longitude, 0.8333° latitude, and 12 unevenly spaced (with respect to altitude) vertical levels with an upper boundary of 100 hPa (Collins et al., 1997; Utembe et al., 2010). In each parcel, the trace gases in the model undergo chemical processes. The chemical processes that occur within the parcel, together with emission, dry and wet deposition, mixing and removal processes are generally uncoupled from transport processes to enable local determination of the timestep (Cooke et al., 2010a,b; Utembe et al., 2010). A detailed description of the vertical coordinate, advection scheme, and dispersion processes used in the STOCHEM can be found in Collins et al. (1997) with updates described by Derwent et al. (2008). The chemical mechanism used in the current version of STOCHEM, is the Common Representative Intermediates mechanism version 2 and reduction 5 (CRI v2-R5), referred to as

'STOCHEM-CRI'. The CRI v2-R5 chemical mechanism was developed on a compound-by-compound basis using 5 day box model simulations with the performance of the chemistry for each compound being compared and optimised with the master chemical mechanism (MCM) with ozone production being the primary criterion (Cooke, 2010). The detail of the CRI v2-R5 mechanism is given by Watson et al. (2008) with updates highlighted in Jenkin et al. (2008) and Utembe et al. (2009, 2010). The mechanism consists of methane and 27 emitted non-methane hydrocarbons using 229 chemical species competing in 627 reactions and gives excellent agreement with the MCM v3.1 over a full range of NO_x levels (Watson et al., 2008; Jenkin et al., 2008). The base case emissions data used in STOCHEM-CRI were adapted from the Precursor of Ozone and their Effects in the Troposphere (POET) inventory (Granier et al., 2005) for the year 1998.

2.2. Scenarios

In this study, the base case experiment performed for the present day was based on the reference conditions described in Utembe et al. (2010) and a model including the isoprene HO_x recycling mechanisms referred to as 'ISOP' is described in detail in Archibald et al. (2010). Experiments were also conducted for a pre-industrial scenario (ca. 1800 AD), representative of an atmosphere devoid of human induced effects, where anthropogenic emissions were completely removed from the model and the reductions in biomass burning emissions are aimed at removing the majority of human induced effects. Several modelling studies that centre on changes in the oxidising capacity of the troposphere from pre-industrial times to the present day have already been reported. However, these have focused primarily on changes in the O_3 burden (Brasseur et al., 1998; Wang and Jacob, 1998; Gauss et al., 2006; Wild and Palmer, 2008); therefore the global burden of ROOH at pre-industrial times produced by the STOCHEM-CRI provide a new dimension to assess the role of human and climatic influences on the troposphere from pre-industrial times. A detailed description of the pre-industrial scenario with the global emissions used in the STOCHEM-CRI can be found in Cooke (2010). All simulations were conducted with meteorology from 1998 for a period of 24 months with the first 12 allowing the model to spin up. Analysis is performed on the subsequent 12 months of data.

3. Results and discussion

3.1. ROOH budget

Table 1 shows the global burden of ROOH (in Tg) produced by the STOCHEM-CRI model for both present and pre-industrial scenarios. It should be noted that the ROOH species include some peroxycarboxylic acids (i.e. of generic formula RC(O)OOH or RCO_3H), which are formed from the reactions of HO_2 with acyl peroxy radicals (RCO_3). The abundance of ROOH simulated using STOCHEM-CRI was found to be greater than that simulated using the previous version of the model (Collins et al., 1997), containing the original chemistry mechanism (referred to here as STOCHEM-OC). This is mainly because the increased complexity of the emitted VOC speciation represented in STOCHEM-CRI is accompanied by a greater input of organic material into the model (e.g. the emissions of monoterpenes). But, there is a large decrease in global burden of methyl hydroperoxide (MHP, CH_3OOH) when using the CRI v2-R5 chemistry (STOCHEM-OC = 2.3 Tg; STOCHEM-CRI = 0.47 Tg) (Cooke, 2010). Because RO_2 radical cross reactions are represented in STOCHEM-CRI, but not in STOCHEM-OC, only 25% of methyl peroxy radicals are removed by forming MHP relative to 35% for the STOCHEM-OC resulting in a reduction on MHP

Table 1
Global burdens of ROOH species for present and pre-industrial scenarios. All values are in Tg.

ROOH species[a]	Total number of ROOH	Present	Preindustrial
CH_3OOH	1	0.469	0.255
Small specific ROOH (C_2–C_3)[b]	3	0.06	0.023
Other ROOH[c]	15	0.214	0.1486
Isoprene degradation ROOH[d]	5	0.814	1.11
α-pinene degradation ROOH[e]	8	0.496	0.641
β-pinene degradation ROOH[f]	4	0.069	0.077
Aromatic hydrocarbon degradation ROOH[g]	3	0.0018	0.00012
Peroxycarboxylic acid (RCO_3H)[h]	3	1.711	1.526
Total ROOH	**42**	**3.83**	**3.78**

[a] More detailed information on ROOH species can be found in Appendix A.
[b] These species are C_2H_5OOH, i-C_3H_7OOH and HOC_2H_4OOH, and are formed from the degradation of many VOCs in the model.
[c] Formed from the degradation of many emitted $\geq C_3$ VOCs.
[d] Only formed from isoprene degradation.
[e] Only formed from α-pinene degradation.
[f] Only formed from β-pinene degradation.
[g] Only formed from aromatic hydrocarbon degradation.
[h] These species are CH_3CO_3H, $HOCH_2CO_3H$ and $C_2H_5CO_3H$, and are formed from the degradation of many VOCs in the model.

formation. Additionally, nitrogen reservoir species (NO_z) are more fully represented in STOCHEM-CRI compared with STOCHEM-OC, which leads to an increase in the NO_x concentration in the free troposphere. The increased NO competes with MHP formation (by reacting with both precursors HO_2 and RO_2) resulting in a decrease in global burden of MHP.

In STOCHEM-CRI, ROOH is formed exclusively from the reaction of organic peroxy radicals (RO_2) with hydroperoxy radicals (HO_2). MHP is the largest single ROOH and is formed by the reaction between CH_3O_2 and HO_2 with 53% of CH_3O_2 radicals formed by the oxidation of methane. In the present day scenario, the removal of MHP is predominantly via reaction with OH (92.1%), photolysis (1.7%), wet deposition (5.4%), and dry deposition (0.8%). After averaging the individual sinks for all ROOH, we have found that the removal of ROOH is dominated by OH (95.2%) followed by photolysis (4.5%). Similar removal results for MHP (with OH (91.8%), photolysis (1.7%), wet deposition (5.6%), dry deposition (0.9%)) and for other ROOH (with OH (94.4%), photolysis (5.2%)) are found for the pre-industrial scenario. Some other dominant ROOH species found in this study are the peroxycarboxylic acids (particularly CH_3CO_3H and $HOCH_2CO_3H$) and isoprene derived hydroperoxides, particularly RU14OOH, RU12OOH, and RU10OOH (see Appendix A for identities).

3.2. Surface distribution of ROOH

The surface distribution of ROOH in December-January-February (D-J-F) and June-July-August (J-J-A) for present day is shown in Fig. 1a. Peak ROOH in December-January-February is observed over South America (up to 7 ppb), southern Africa (up to 4 ppb), and north Australia (up to 4 ppb) as a result of biomass burning and the large emissions of VOCs (e.g. isoprene, terpenes). In J-J-A, the peak ROOH is found over southern Africa and South America, but there are also substantial abundances of ROOH (up to 2 ppb) over North America, central Europe and South East Asia because of increased photochemical production in the northern hemisphere summer. In summer time, the peak solar flux is located at about 20°N and thus the photochemistry between 30°N and 60°N is more rapid than in winter time resulting in high levels of ROOH in the northern hemisphere. There is no significant differences between the surface distribution of ROOH for pre-industrial

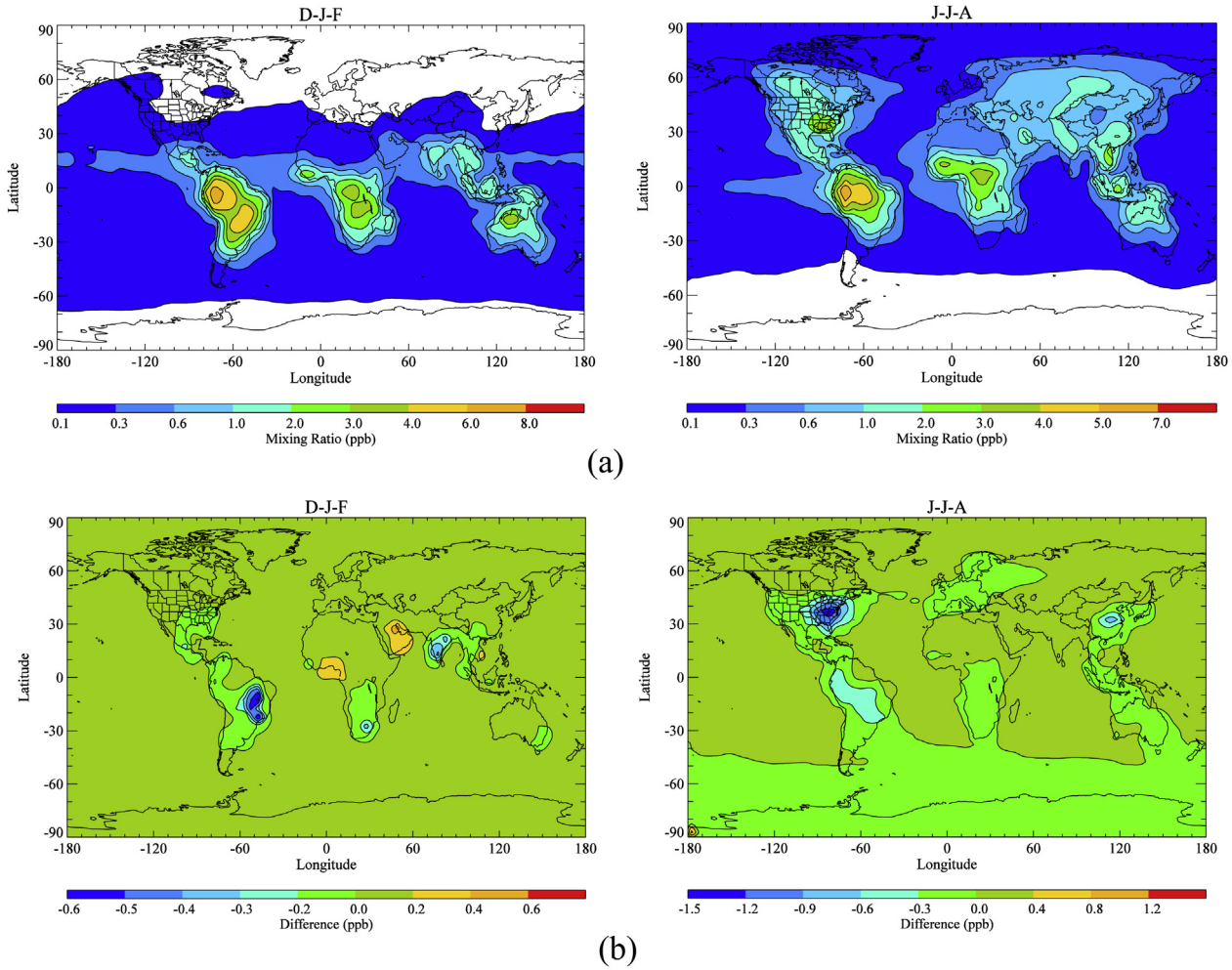

Fig. 1. (a) Annual mean surface level distribution of ROOH for D-J-F and J-J-A months in the present scenario, (b) annual surface layer ROOH difference between present and pre-industrial scenarios (Note: difference = (Present−Preindustrial).

and present day simulation, both having similar magnitude mixing ratios (see Fig 1b). Compared with the preindustrial scenario, the higher CO and VOCs in the present day scenario favours the formation of HO_2 (1.8×10^{38} molecules y^{-1} for present and 1.0×10^{38} molecules y^{-1} for pre-industrial) and RO_2 (1.9×10^{38} molecules y^{-1} for present and 9.9×10^{37} molecules y^{-1} for pre-industrial), respectively resulting in a 2-fold increase in production of ROOH, but higher NO_x reacts with RO_2 and HO_2 (2.3×10^{38} molecules y^{-1} for present and 1.2×10^{38} molecules y^{-1} for pre-industrial), resulting in a 2-fold suppression of ROOH formation via reaction (R1).

The zonal distribution of ROOH shows a peak at the surface just south of the equator where there are large emissions of VOCs from forested areas, increased biomass burning, and higher levels of photochemical activity (Fig. 2a). ROOH concentrations decrease with increasing altitude, but a significant amount of ROOH (0.4 ppb) still exists at approximately 14 km in the model. The acyl peroxy radicals (e.g. CH_3CO_3, $C_2H_5CO_3$, and $HOCH_2CO_3$) are ubiquitously distributed throughout the troposphere because of their formation during the oxidation of most NMVOCs which can react with HO_2 to produce RCO_3H in the upper troposphere. A slight increase (up to 0.15 ppb) of the zonal average distribution of ROOH are found from pre-industrial to the present day simulation (Fig 2b).

3.3. Evaluation using atmospheric measurements

The data compilation of Emmons et al. (2000) and Wang et al. (2001, 2003) containing measurements of CH_3OOH from a series of flight campaigns was used to evaluate the STOCHEM-CRI model of CH_3OOH and ROOH. Emmons et al. (2000) and Wang et al. (2001, 2003) described the methodology which was used to produce average values over a given region and assessed the use of flight measurement data for model evaluation. Reasonable agreement between measurement data and our model data is found (See Fig. 3).

In the lower troposphere (0–4 km), the mean bias of CH_3OOH from measurements for all locations is −0.50 ppbv and in the upper troposphere (6–10 km), the mean bias from measurements is −0.12 ppbv. Therefore, the STOCHEM-CRI underpredicts CH_3OOH, largely in the lower troposphere. The ROOH levels produced by the model are 2–5 times higher than model CH_3OOH levels (See Fig. 3). The model is driven by meteorology for the year 1998 and therefore when comparing with measurement data from other years, consideration of inter-annual variation give more reliable agreement between measurement and model data. 1998 was an El-Niño year which could lead to additional differences especially when compared with transition and La-Niña years. However, the measured values may not represent the mean state of

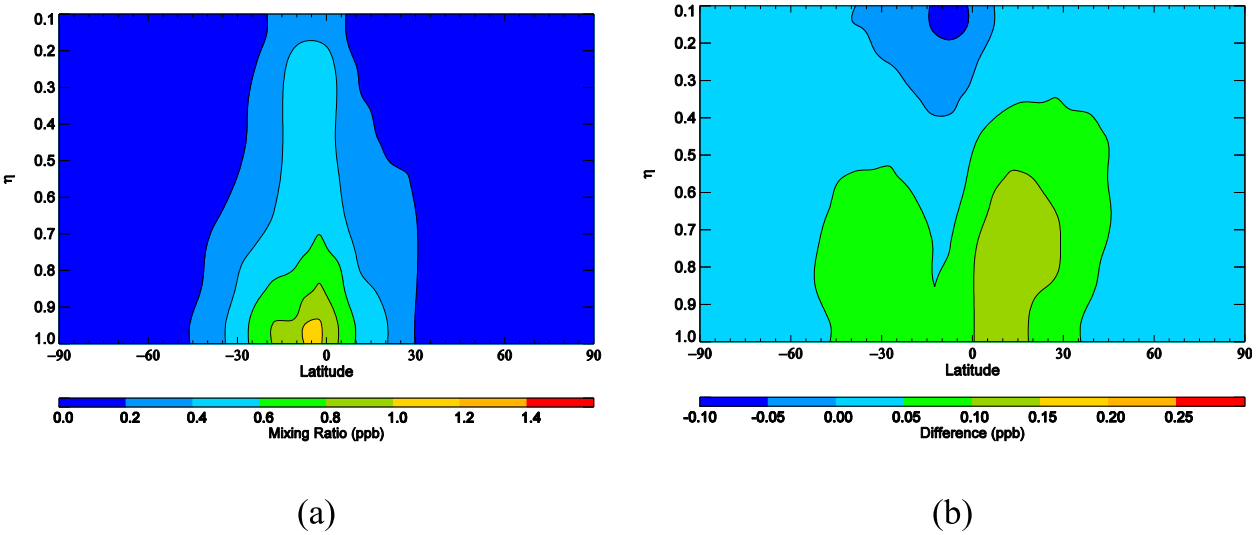

Fig. 2. (a) Annual mean zonal average distribution of ROOH in the present scenario, (b) annual zonal average distribution of ROOH difference between present and pre-industrial scenarios (Note: difference = (Present−Preindustrial).

the region because of unusual meteorology. The coarse emission grids in STOCHEM make the evaluation with sites near strong source regions difficult. The surface sites measure a range of polluted and background air masses, depending on the meteorology, which makes comparison with a background global Chemistry Transport Model (CTM) problematic. Nevertheless, comparison is worthwhile and will highlight not only inevitable deficiencies in the model formulation (true of all models) but also potential deficiencies in chemistry and emissions.

3.4. Seasonality of ROOH

The twelve surface measurement campaigns selected for model evaluation are presented in Table 2. The levels of modelled ROOH at 12 surface stations throughout the 1998 calendar year exhibit a strong seasonal correlation (Fig. 4). During the summer months, the levels of ROOH are at their highest, peaking in July or August. Minimum levels of ROOH are found during the winter season. The Cape Grim and Antarctica stations show an opposite but an analogous seasonal trend in the Southern Hemisphere with maximum and minimum values recorded in July and January, respectively.

Photochemical activity is likely to be the determining factor of the seasonal variations of the ROOH abundances in the atmosphere. For both hemispheres, peak ROOH is calculated to occur in summer when photochemical sources of free radicals are at a maximum. The calculated changes in ROOH levels at the tropical region station, Mauna Loa, throughout the progression of seasons are much smaller than in the other stations. The seasonal changes in both sunlight and temperature are relatively small at Mauna Loa and therefore the seasonal cycle consists of a series of non-descript peaks and troughs in an analogous manner to the O_3 concentration–time profile. The ROOH peak is calculated to be in March at the Mauna Loa surface station. This feature can be attributed to an increased flux of O_3 from the stratosphere to the troposphere as a result of increased stratosphere–troposphere exchange (STE) (Kirgis et al., 2012). Another ROOH peak during summer time can be explained by the higher OH concentration resulting in higher peroxy radicals.

The average monthly model data of ROOH during 1998 are compared with the field measurement data of the equivalent months for the selected stations (Fig. 4). Except Pabstthum, all field measurements were reported during years other than 1998. The comparison shows that our model values yield lower ROOH abundances than the field campaign values for most of the stations (See Fig. 4). These data output by the model are averaged over a 5° latitude × 5° longitude grid square whereas the measurement stations record data at a specific location. However, the difference between the model and the measurement data are reasonable for most of the stations (e.g. Oku-Nikko, Mount Tai, Beijing, Portugal, Mauna Loa, Pabstthum, Hong Kong, and Mace Head). The large difference between the measurement and the model data are found for Cape Grim, Southern Switzerland, Antarctica, and Greenland summer campaigns. A summer campaign does represent the extreme conditions (e.g. highest photolytic activity, large vegetative emissions, biomass burning) for their representative months, and so it may well be that the model will struggle to reproduce such values. The duration of the field campaigns varies from days to a few months affecting ROOH abundances due to different air mass (e.g. clean, polluted, semi-polluted) arriving at the location-this causes difficulties when making comparisons between measurement and modelled data, as the modelled data are instead averaged over 25 days. Much research into the photochemistry above ice surfaces has taken place and revealed a series of interesting results where photolysis of nitrate in ice can lead to significant emissions of NO_x (e.g. Grannas et al., 2007). Hence a pristine environment where ozone loss is expected can be a very different environment. Such subtleties are not included in these simulations and so it is not surprising that the global model departs from measurements most notably in such environments.

3.5. Impacts on ROOH of including additional HO_x recycling mechanisms

The role of mechanisms that increase the efficiency of HO_x recycling in the troposphere has been an important consideration in recent times, particularly in relation to isoprene oxidation (e.g. Lelieveld et al., 2008; Peeters et al., 2009; Paulot et al., 2009; Fuchs et al., 2013). Accordingly, Archibald et al. (2010) have previously implemented additional HO_x recycling mechanisms into STOCHEM-CRI, benchmarked against more detailed representations implemented into MCM v3.1. The mechanisms included a reduced representation of HO_x recycling resulting from

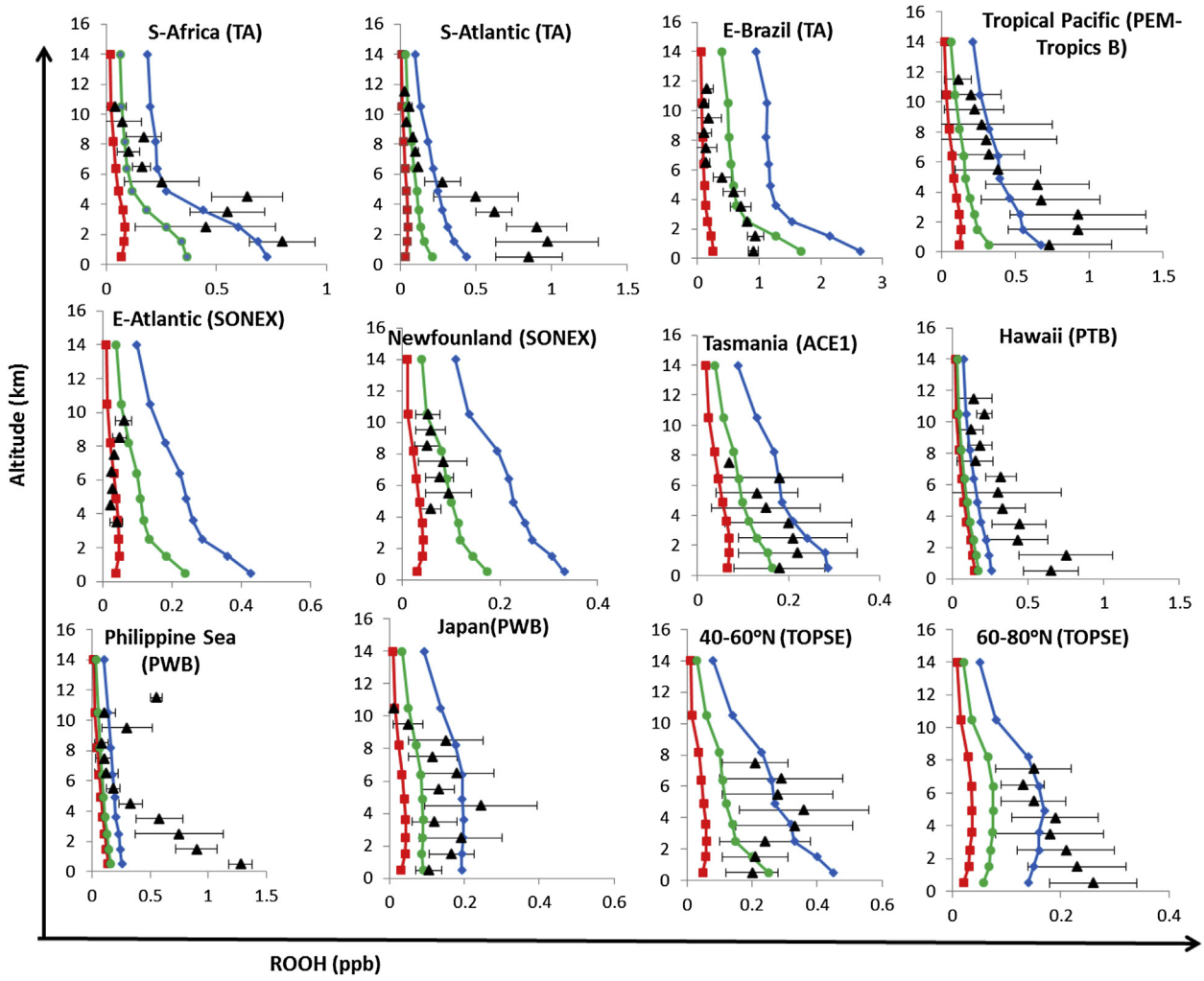

Fig. 3. Vertical profiles for measured and calculated ROOH, using the aircraft measurement compilations from Emmons et al. (2000) and the STOCHEM-CRI calculations. Red, blue and green lines represent mean calculated values of CH_3OOH, ROOH, and ROOH after excluding RCO_3H, respectively over the period of the campaign for base model. Black triangles represent the measurement CH_3OOH data and the black error bars represent measurement variability. (For interpretation of the references to color in this figure caption, the reader is referred to the web version of this article.)

Table 2
Details of the respective locations analysed in the model study, and the year in which they were conducted.

Location	Latitude	Longitude	Year	Source
Greenland	73°N	39°W	2003–04	Frey et al., 2009
Portugal	40°N	1°E	1994	Jackson and Hewitt, 1996
Mace Head	53°N	10°W	1998–99	Morgan and Jackson, 2002
Beijing	40°N	116°E	2006–08	Zhang et al., 2012
Hong Kong	22°N	114°E	2011–12	Guo et al., 2014
Mauna Loa	19°N	156°W	1988	Heikes, 1992
Cape Grim	41°S	145°E	1991	Ayers et al., 1996
Mount Tai	36°N	117°E	2007	Ren et al., 2009
Oku-Nikko	36°N	139°E	2000	Takami et al., 2003
Southern Switzerland	45°N	9°W	1994	Staffelbach et al., 1997
Pabstthum, Germany	53°N	13°E	1998	Grossmann et al., 2003
West Antarctica	76°S to 79°S	89°W to 103°W	2001	Frey et al., 2005

The peroxidase-catalysed dimerization of *p*-hydroxyphenylacetic acid with fluorometric detection technique was used for all measurements.

isomerisation of isoprene-derived peroxy radicals (based on Peeters et al., 2009), which is isoprene-specific; and the inclusion of propagating channels for the reactions of HO_2 with acyl peroxy radicals (e.g. Hasson et al., 2004, 2012; Jenkin et al., 2007; Dillon and Crowley, 2008), which influences HO_x recycling from VOC oxidation in general. Here we compare the base case integrations with those where the additional HO_x recycling mechanism have been included.

The percentage change in total ROOH between the base and the additional HO_x recycling runs for both present and pre-industrial scenarios is shown in Fig. 5a. The results follow the same general pattern for both scenarios, with the greatest percentage changes

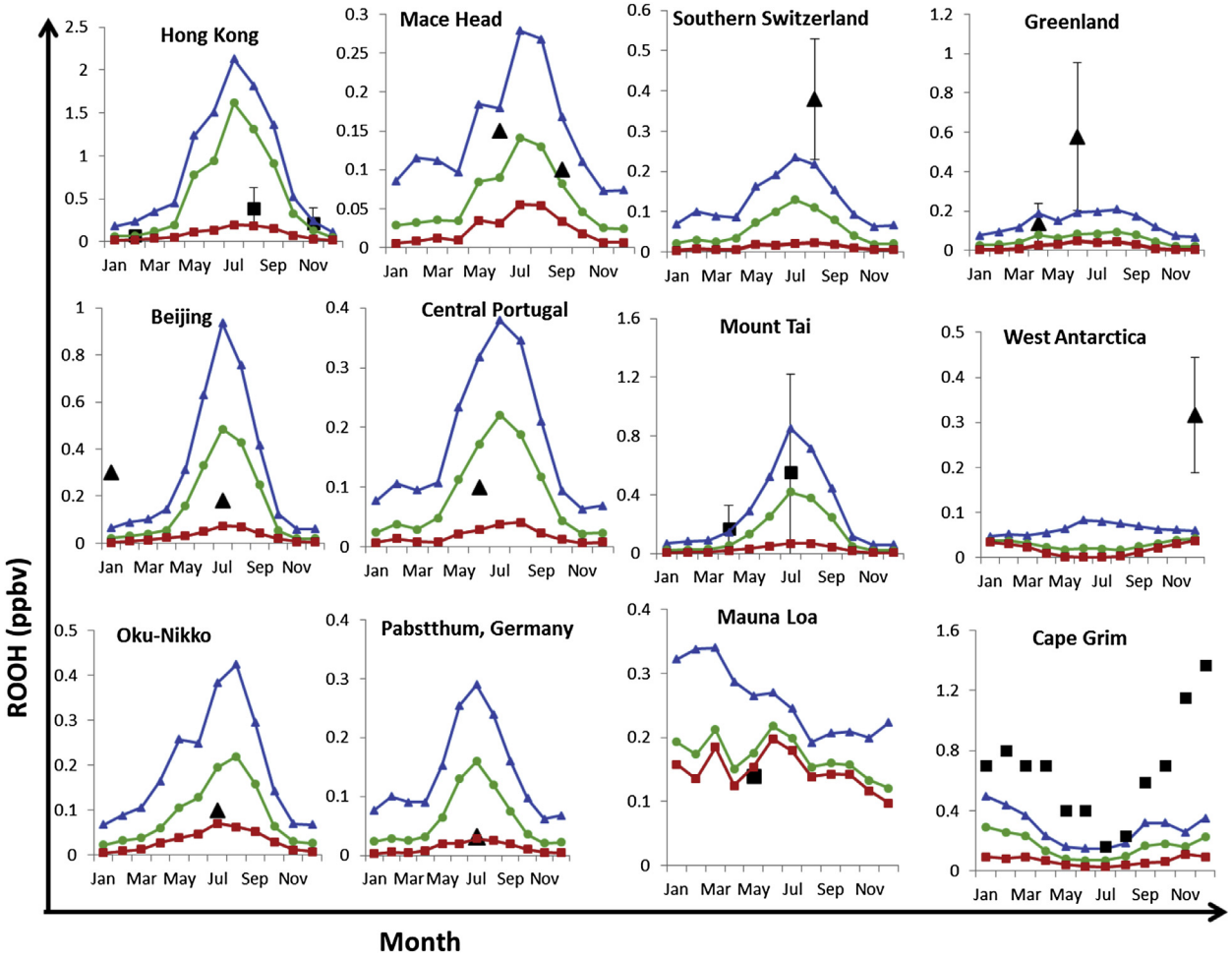

Fig. 4. Monthly variation of the surface ROOH abundances of selected monitoring stations produced by the STOCHEM-CRI. Red, blue and green lines represent mean calculated values of CH_3OOH, ROOH, and ROOH after excluding RCO_3H, respectively, black square symbols represent the measurement data of ROOH and black triangle symbols represent the measurement data of CH_3OOH. (For interpretation of the references to color in this figure caption, the reader is referred to the web version of this article.)

over the tropical forested regions where isoprene emissions are large. In the present day scenario, CH_3OOH abundances are increased by up to 80% (see Fig. 5b) and total ROOH abundances by up to 30% (see Fig. 5a). This is mainly due to the general increasing effect on HO_2 and RO_2 levels that results from operation of the additional HO_x recycling mechanisms in isoprene-rich regions at low NO_x levels (e.g. as illustrated by Archibald et al., 2010). In the pre-industrial scenario, the increases in CH_3OOH and total ROOH abundances are even larger (up to 110% and 40%, respectively), reflecting the more efficient operation of the HO_x recycling mechanisms at lower NO_x levels. Since the pioneering work of Peeters et al. (2009), subsequent investigations have suggested that the efficiency of HO_x recycling from the isoprene peroxy radical isomerisation mechanism is almost certainly lower than originally estimated (e.g. Archibald et al., 2010; Crounse et al., 2011; Peeters et al., 2014). Nevertheless, the present work provides an estimate of the upper limit for impact of the mechanism on ROOH abundances.

In the specific cases of the peroxycarboxylic acids, RCO_3H (represented here by CH_3CO_3H, $C_2H_5CO_3H$ and $HOCH_2CO_3H$), implementation of the HO_x recycling mechanisms results in decreases in their total abundance of up to 30% over tropical forested regions in the present and pre-industrial scenarios (see Fig. 5c). The RCO_3H species are formed specifically from terminating channels of the reactions of HO_2 with acyl peroxy radicals (RCO_3), via reaction (R11a), such that the implementation of propagating channels (reaction (R11b)) for these reactions has a direct reducing impact on their formation:

$$RCO_3 + HO_2 \rightarrow RCO_3H + O_2 \quad \text{(R11a)}$$

$$RCO_3 + HO_2 \rightarrow RCO_2 + OH + O_2 \quad \text{(R11b)}$$

$$RCO_2\,(+O_2) \rightarrow RO_2 + CO_2 \quad \text{(R12)}$$

This leads to a net reduction in the abundance of RCO_3H, even though the levels of both RCO_3 and HO_2 are generally increased by the elevated efficiency of HO_x recycling resulting from implementation of both the mechanisms considered here.

As shown in Fig. 5c, even greater percentage reductions in RCO_3H abundances (up to 70%) are simulated in other regions, leading to global reductions of almost 50% in both the present day and pre-industrial scenarios. This also has a notable reducing impact on total ROOH burdens over large areas of the globe, resulting in overall global reductions in total ROOH of 23% and 20% in the present day and pre-industrial scenarios, respectively. However, if RCO_3H species are excluded from the total, implementation of the additional HO_x recycling mechanisms leads to almost no change in the global abundance of ROOH in either scenario.

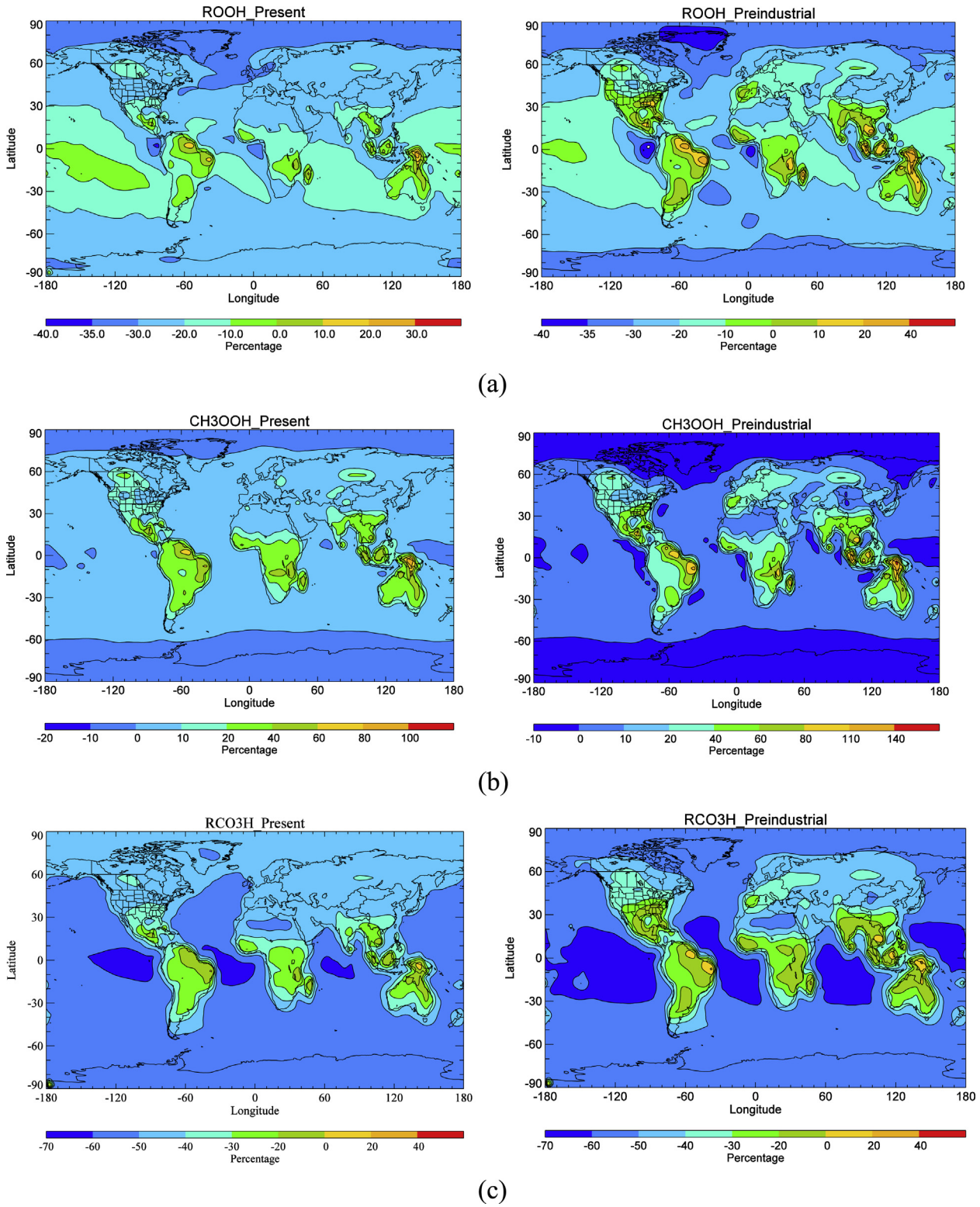

Fig. 5. The percentage changes of annual ROOH from ISOP to base run for present and pre-industrial scenarios, (a) ROOH, (b) CH_3OOH, (c) RCO_3H. Note that percentage change (%) = ((ISOP−base)*100)/base.

4. Conclusion

The oxidation of VOCs leads to the formation of RO_2, RO, and HO_2 which act as chain propagation species. Under NO_x-limited conditions (i.e. high [VOC]/[NO_x]), the reaction between RO_2 and HO_2 dominates RO_2 removal, leading to the preferential formation of ROOH. The highest ROOH abundances (up to 7 ppb) are simulated over the tropical forested areas of South America, due to the large emissions of VOCs (e.g. isoprene, terpenes) and the low NO_x levels. Maximum ROOH abundances in the summer months

coincide with maximum temperature and solar intensity responsible for the highest photochemical production and higher VOC emission. A wide range of observations of ROOH during aircraft and field campaigns conducted between 1991 and 2008 were used to evaluate the chemical scheme and dynamic core that characterise the STOCHEM-CRI model. Inevitable differences between measurements and model data arose, with the model's parameterised approach generally underpredicting ROOH abundances in relation to the levels recorded in the field campaigns. The vertical distribution of CH_3OOH from our model study underpredicts measured values by a factor of 2–5 in lower troposphere, the adoption of a higher emission grid resolution would, in our opinion, improve the model simulations and comparisons between modelled and field data. A significant amount of ROOH is found in the upper troposphere, which is driven by acyl peroxy radicals. In the pre-industrial scenario, the lower NO_x encountered promotes the permutation reactions of peroxy radicals, but the lower anthropogenic emissions of VOCs decrease the production of RO_2, these two opposite effects lead to almost no change in the global abundance of ROOH when we compare with the present day simulation. The effects of HO_x recycling mechanisms caused significant increases in CH_3OOH and ROOH (up to 80% and 30%, respectively for present day simulation) and (up to 110% and 40%, respectively for pre-industrial scenario) over tropical forested regions.

Acknowledgement

ATA thanks GWR and the U.K. Met. Office for funding (studentship), MCC thanks EPSRC for a studentship, DES and CJP thank NERC and Bristol ChemLabS under whose auspices various aspects of this work was funded.

Appendix A. Supplementary data

Supplementary data related to this article can be found at http://dx.doi.org/10.1016/j.atmosenv.2015.03.045.

References

Archibald, A.T., Cooke, M.C., Utembe, S.R., Shallcross, D.E., Derwent, R.G., Jenkin, M.E., 2010. Impacts of mechanistic changes on HO_x formation and recycling in the oxidation of isoprene. Atmos. Chem. Phys. 10, 8097–8118.

Ayers, G.P., Penkett, S.A., Gillett, R.W., Bandy, B., Galbally, I.E., Meyer, C.P., Elsworth, C.M., Bentley, S.T., Forgan, B.W., 1996. The annual cycle of peroxides and ozone in marine air at Cape Grim, Tasmania. J. Atmos. Chem. 23, 221–252.

Brasseur, G.P., Kiehl, J.T., Muller, J.F., Schneider, T., Granier, C., Tie, X.X., Hauglustaine, D., 1998. Past and future changes in global tropospheric ozone: impact on radiative forcing. Geophys. Res. Letts 25, 3807–3810.

Brune, W.H., Faloona, I.C., Tan, D., Weinheimer, A.J., Campos, T., Ridley, B.A., Vay, S.A., Collins, J.E., Sachse, G.W., Jaeglé, L., Jacob, D.J., 1998. Airborne in situ OH and HO_2 observations in the cloud-free troposphere and lower stratosphere during SUCCESS. Geophys. Res. Lett. 25, 1701–1704.

Chen, Z.M., Wang, H.L., Zhu, L.H., Wang, C.X., Jie, C.Y., Hua, W., 2008. Aqueous-phase ozonolysis of methacrolein and methyl vinyl ketone: a potentially important source of atmospheric aqueous oxidants. Atmos. Chem. Phys. 8, 2255–2265.

Cohan, D.S., Schultz, M.G., Jacob, D.J., 1999. Convective injection and photochemical decay of peroxides in the tropical upper troposphere: methyl iodide as a tracer of marine convection. J. Geophys. Res. 104, 5717–5724.

Collins, W.J., Stevenson, D.S., Johnson, C.E., Derwent, R.G., 1997. Tropospheric ozone in a global-scale three-dimensional Lagrangian model and its response to NO_x emission controls. J. Atmos. Chem. 26 (3), 223–274.

Cooke, M.C., Utembe, S.R., Carbajo, P.G., Archibald, A.T., Orr-Ewing, A.J., Derwent, R.G., Jenkin, M.E., Shallcross, D.E., 2010a. Impacts of formaldehyde photolysis rates on tropospheric chemistry. Atmos. Sci. Lett. 11, 33–38.

Cooke, M.C., Marven, A.R., Utembe, S.R., Archibald, A.T., Ensor, G.W.R., Jenkin, M.E., Derwent, R.G., O'Doherty, S.J., Shallcross, D.E., 2010b. On the effect of a global adoption of various fractions of biodiesel on key species in the troposphere. Int. J. Oil Gas. Coal Tech. 3, 88–103.

Cooke, M.C., 2010. Global Modelling of Atmospheric Trace Gases using the CRI Mechanism (PhD thesis). University of Bristol, UK.

Crounse, J.D., Paulot, F., Kjaergaard, H.G., Wennberg, P.O., 2011. Peroxy radical isomerization in the oxidation of isoprene. Phys. Chem. Chem. Phys. 13, 13607–13613.

Derwent, R.G., Stevenson, D.S., Doherty, R.M., Collins, W.J., Sanderson, M.G., 2008. How is surface ozone in Europe linked to Asian and North American NO_x emissions? Atmos. Environ. 42, 7412–7422.

Dillon, T.J., Crowley, J.N., 2008. Direct detection of OH formation in the reactions of HO_2 with $CH_3C(O)O_2$ and other substituted peroxy radicals. Atmos. Chem. Phys. 8 (16), 4877–4889.

Emmons, L.K., Hauglustaine, D.A., Müller, J.-F., Carroll, M.A., Brasseur, G.P., Brunner, D., Staehelin, J., Thouret, V., Marenco, A., 2000. Data composites of airborne observations of tropospheric ozone and its precursors. J. Geophys. Res. 105, 20497–20538.

Frey, M.M., Stewart, R.W., McConnell, J.R., Bales, R.C., 2005. Atmospheric hydroperoxides in west Antarctica: links to stratospheric ozone and atmospheric oxidation capacity. J. Geophys. Res. 110, D23301.

Frey, M.M., Hutterli, M.A., Chen, G., Sjostedt, S.J., Burkhart, J.F., Friel, D.K., Bales, R.C., 2009. Contrasting atmospheric boundary layer chemistry of methylhydroperoxide (CH_3OOH) and hydrogen peroxide (H_2O_2) above polar snow. Atmos. Chem. Phys. 9, 3261–3276.

Fuchs, H., Hofzumahaus, A., Rohrer, F., Bohn, B., Brauers, T., Dorn, H.-P., Häseler, R., Holland, F., Kaminski, M., Li, X., Lu, K., Nehr, S., Tillmann, R., Wegener, R., Wahner, A., 2013. Experimental evidence for efficient hydroxyl radical regeneration in isoprene oxidation. Nat. Geosci. 6, 1023–1026.

Gauss, M., Myhre, G., Isaksen, I.S., Grewe, V., Pitari, G., Wild, O., Collins, W.J., Dentener, F.J., Ellingsen, K., Gohar, K.L., Hauglustaine, D.A., Iachetti, D., Lamarque, F., Mancini, E., Mickley, L.J., Prather, M.J., Pyle, J.A., Sanderson, M.J., Shine, K.P., Stevenson, D.S., Sudo, K., Szopa, S., Zeng, G., 2006. Radiative forcing since preindustrial times due to ozone change in the troposphere and the lower stratosphere. Atmos. Chem. Phys. 6, 575–599.

Granier, C., Lamarque, J.F., Mieville, A., Muller, J.F., Olivier, J., Orlando, J., Peters, J., Petron, G., Tyndall, G., Wallens, S., 2005. POET, a Database of Surface Emissions of Ozone Precursors. http://www.aero.jussieu.fr/project/ACCENT/POET.php.

Grannas, A.M., Jones, A.E., Dibb, J., Ammann, M., Anastasio, C., Beine, H.J., Bergin, M., Bottenheim, J., Boxe, C.S., Carver, G., Chen, G., Crawford, J.H., Dominé, F., Frey, M.M., Guzmán, M.I., Heard, D.E., Helmig, D., Hoffmann, M.R., Honrath, R.E., Huey, L.G., Hutterli, M., Jacobi, H.W., Klán, P., Lefer, B., McConnell, J., Plane, J., Sander, R., Savarino, J., Shepson, P.B., Simpson, W.R., Sodeau, J.R., von Glasow, R., Weller, R., Wolff, E.W., Zhu, T., 2007. An overview of snow photochemistry: evidence, mechanisms and impacts. Atmos. Chem. Phys. 7, 4329–4373.

Grossmann, D., Moortgat, G.K., Kibler, M., Schlomski, S., Bachmann, K., Alicke, B., Geyer, A., Platt, U., Hammer, M.U., Vogel, B., Mihelcic, D., Hofzumahaus, A., Holland, F., Volz-Thomas, A., 2003. Hydrogen peroxide, organic peroxides, carbonyl compounds, and organic acids measured at Pabstthum during BERLIOZ. J. Geophys. Res. 108, 8250.

Gunz, D.W., Hoffmann, M.R., 1990. Atmospheric chemistry of peroxides: a review. Atmos. Environ. 24A, 1601–1633.

Guo, J., Tilgner, A., Yeung, C., Wang, Z., Louie, P.K.K., Luk, C.W.Y., Xu, Z., Yuan, C., Gao, Y., Poon, S., Herrmann, H., Lee, S., Lam, K.S., Wang, T., 2014. Atmospheric peroxides in a polluted subtropical environment: seasonal variation, sources and sinks, and importance of heterogeneous processes. Environ. Sci. Technol. 48, 1443–1450.

Hasson, A.S., Tyndall, G.S., Orlando, J.J., Singh, S., Hernandez, S.Q., Campbell, S., Ibarra, Y., 2012. Branching ratios for the reaction of selected carbonyl-containing peroxy radicals with hydroperoxy radicals. J. Phys. Chem. A 116, 6264–6281.

Hasson, A.S., Tyndall, G.S., Orlando, J.J., 2004. A product yield study of the reaction of HO_2 radicals with ethyl peroxy ($C_2H_5O_2$), acetyl peroxy ($CH_3C(O)O_2$), and acetonyl peroxy ($CH_3C(O)CH_2O_2$) radicals. J. Phys. Chem. A 108 (28), 5979–5989.

He, S.Z., Chen, Z.M., Zhang, X., Zhao, Y., Huang, D.M., Zhao, J.N., Zhu, T., Hu, M., Zeng, L.M., 2010. Measurement of atmospheric hydrogen peroxide and organic peroxides in Beijing before and during the 2008 olympic games: chemical and physical factors influencing their concentrations. J. Geophys. Res. 115, D17307.

Heikes, B.G., 1992. Formaldehyde and hydroperoxides at mauna loa observatory. J. Geophys. Res. 97, 18001–18013.

Heikes, B., Lee, M., Jacob, D., Talbot, R., Bradshaw, J., Singh, H., Blake, D., Anderson, B., Fuelberg, H., Thompson, A.M., 1996. Ozone, hydroperoxide, oxides of nitrogen, and hydrocarbon budgets in the marine boundary layer over the South Atlantic. J. Geophys. Res. 101, 24221–24234.

Hewitt, C.N., Kok, G.L., Fall, R., 1990. Hydroperoxides in plants exposed to ozone mediate air pollution damage to alkene emitters. Nature 344, 56–58.

Hewitt, C.N., Kok, G.L., 1991. Formation and occurrence of organic hydroperoxides in the troposphere: laboratory and field observations. J. Atmos. Chem. 12, 181–194.

Hewitt, C.N., Terry, G., 1992. Understanding plant-ozone interactions. Environ. Sci. Technol. 26, 1890–1891.

Horie, O., Neeb, P., Limbach, S., Moortgat, G.K., 1994. Formation of formic acid and organic peroxides in the ozonolysis of ethene with added water vapour. Geophys. Res. Lett. 21, 1523–1526.

Hua, W., Chen, Z.M., Jie, C.Y., Kondo, Y., Hofzumahaus, A., Takegawa, N., Chang, C.C., Lu, K.D., Miyazaki, Y., Kita, K., Wang, H.L., Zhang, Y.H., Hu, M., 2008. Atmospheric hydrogen peroxide and organic hydroperoxides during PRIDE-PRD'06, China: their concentration, formation mechanism and contribution to secondary aerosols. Atmos. Chem. Phys. 8 (22), 6755–6773.

Jackson, A.V., Hewitt, C.N., 1996. Hydrogen peroxide and organic hydroperoxide concentrations in air in a eucalyptus forest in central Portugal. Atmos. Environ 30, 819–830.

Jaeglé, L., Jacob, D.J., Wennberg, P.O., Spivakovsky, C.M., Hanisco, T.F.,

Lanzendorf, E.J., Hintsa, E.J., Fahey, D.W., Keim, E.R., Proffitt, M.H., Atlas, E.L., Flocke, F., Schauffler, S., McElroy, C.T., Midwinter, C., Pfister, L., Wilson, J.C., 1997. Observed OH and HO_2 in the upper troposphere suggest a major source from convective injection of peroxides. Geophys. Res. Lett. 24, 3181–3184.

Jenkin, M.E., Hurley, M.D., Wallington, T.J., 2007. Investigation of the radical product channel of the $CH_3C(O)O_2 + HO_2$ reaction in the gas phase. Phys. Chem. Chem. Phys. 9 (24), 3149–3162.

Jenkin, M.E., Watson, L.A., Utembe, S.R., Shallcross, D.E., 2008. A Common representative intermediate (CRI) mechanism for VOC degradation. Part-1: gas phase mechanism development. Atmos. Environ. 42, 7185–7195.

Kirgis, G., LeBlanc, T., McDermid, S., Walsh, T.D., 2012. Stratospheric ozone interannual variability (1995-2011) as observed by lidar and satellite at Mauna Loa observatory, HI and table mountain facility, CA. Atmos. Chem. Phys. 13, 5033–5047.

Kleinman, L.I., 1986. Photochemical formation of peroxides in the boundary layer. J. Geophys. Res. 91, 10889–10904.

Kleinman, L.I., 1991. Seasonal dependence of boundary layer peroxide concentrations: the low and the high NO_x regimes. J. Geophys. Res. 96, 20721–20733.

Lee, M., Heikes, B.G., 1997. Hydrogen peroxide, organic hydroperoxide, and formaldehyde as primary pollutants from biomass burning. J. Geophys. Res. 102, 1301–1309.

Lee, M., Heikes, B.G., Jacob, D.J., 1998. Enhancements of hydroperoxides and formaldehyde in biomass impacted air and their effect on atmospheric oxidant cycles. J. Geophys. Res. 103, 13201–13212.

Lelieveld, J., Butler, T.M., Crowley, J.N., Dillon, T.J., Fischer, H., Ganzeveld, L., Harder, H., Lawrence, M.G., Martinez, M., Taraborrelli, D., Williams, J., 2008. Atmospheric oxidation capacity sustained by a tropical forest. Nature 452 (7188), 737–740.

Lightfoot, P.D., Cox, R.A., Crowley, J.N., Destiau, M., Hayman, G.D., Jenkin, M.E., Moortgat, G.K., Zabel, F., 1992. Organic peroxy radicals: kinetics, spectroscopy and tropospheric chemistry. Atmos. Environ. 26, 1805–1961.

Lin, G., Penner, J.E., Sillman, S., Taraborrelli, D., Lelieveld, J., 2012. Global modeling of SOA formation from dicarbonyls, epoxides, organic nitrates and peroxides. Atmos. Chem. Phys. 12, 4743–4774.

Logan, J.A., Prather, M.J., Wofsy, S.C., McElroy, M.B., 1981. Tropospheric chemistry: a global perspective. J. Geophys. Res. 86, 7210–7254.

Madronich, S., Calvert, J.G., 1990. Permutation reactions of organic peroxy-radicals in the troposphere. J. Geophy. Res. 95, 5697–5715.

Mari, C., Jacob, D.J., Bechthold, P., 2000. Transport and scavenging of soluble gases in a deep convective cloud. J. Geophys. Res. 105, 22255–22267.

Morgan, R.B., Jackson, A.V., 2002. Measurements of gas-phase hydrogen peroxide and methyl hydroperoxide in the coastal environment during the PARFORCE project. J. Geophys. Res. 107, 8109.

O'Sullivan, D.W., Heikes, B.G., Lee, M., Chang, C., Gregory, G., Blake, D., Sachse, G., 1999. The distribution of hydrogen peroxide and methyl hydroperoxide in the Pacific and South Atlantic. J. Geophys. Res. 104, 5635–5646.

Paulot, F., Crounse, J.D., Kjaergaard, H.G., Kurten, A., St Clair, J.M., Seinfeld, J.H., Wennberg, P.O., 2009. Unexpected epoxide formation in the gas-phase photooxidation of isoprene. Science 325 (5941), 730–733.

Peeters, J., Nguyen, T.L., Vereecken, L., 2009. HO_x radical regeneration in the oxidation of isoprene. Phys. Chem. Chem. Phys. 11, 5935–5939.

Peeters, J., Müller, J.-F., Stavrakou, T., Nguyen, V.S., 2014. Hydroxyl radical recycling in isoprene oxidation driven by hydrogen bonding and hydrogen tunneling: the upgraded LIM1 mechanism. J. Phys. Chem. A 118 (38), 8625–8643.

Polle, A., Junkermann, W., 1994. Inhibition of apoplastic and symplastic peroxidase activity from Norway spruce by the photooxidant hydroxymethyl hydroperoxide. Plant Physiol. 104, 617–621.

Ravetta, F., Jacob, D.J., Brune, W.H., Heikes, B.G., Anderson, B.E., Blake, D.R., Gregory, G.L., Sachse, G.W., Sandholm, S.T., Shetter, R.E., Singh, H.B., Talbot, R.W., 2001. Experimental evidence for the importance of convected methylhydroperoxide as a source of hydrogen oxide (HO_x) radicals in the tropical upper troposphere. J. Geophys. Res. 106, 32709–32716.

Ren, Y., Ding, A., Wang, T., Shen, X., Guo, J., Zhang, J., Wang, Y., Xu, P., Wang, X., Gao, J., Collett, J.L., 2009. Measurement of gas-phase total peroxides at the summit of mount Tai in China. Atmos. Environ. 43, 1702–1711.

Sakugawa, H., Kaplan, I.R., Tsai, W., Cohen, Y., 1990. Atmospheric hydrogen peroxide; does it share a role with ozone in degrading air quality? Environ. Sci. Technol. 24, 1452–1462.

Simonaitis, R., Olszyna, K.J., Meagher, J.F., 1991. Production of hydrogen peroxide and organic peroxides in the gas phase reactions of ozone with natural alkenes. Geophys. Res. Lett. 18, 9–12.

Snow, J.A., Heikes, B.G., Shen, H.W., O'Sullivan, D.W., Fried, A., Walega, J., 2007. Hydrogen peroxide, methyl hydroperoxide, and formaldehyde over North America and the North Atlantic. J. Geophys. Res. 112, D12s07.

Staffelbach, T., Neftel, A., Blatter, A., Gut, A., Fahrni, M., Stähelin, J., Prévôt Hering, A., Lehning, M., Neininger, B., Bäumle, M., Kok, G.L., Dommen, J., Hutterli, M., Anklin, M., 1997. Photochemical oxidant formation over southern Switzerland 1. Results from summer 1994. J. Geophys. Res. 102 (D19), 23345–23362.

Takami, A., Shiratori, N., Yonekura, H., Hatakeyama, S., 2003. Measurement of hydroperoxides and ozone in Oku-Nikko area. Atmos. Environ. 37, 3861–3872.

Utembe, S.R., Cooke, M.C., Archibald, A.T., Jenkin, M.E., Derwent, R.G., Shallcross, D.E., 2010. Using a reduced common representative intermediates (CRI v2-R5) mechanism to simulate tropospheric ozone in a 3-D Lagrangian chemistry transport model. Atmos. Environ. 13, 1609–1622.

Utembe, S.R., Watson, L.A., Shallcross, D.E., Jenkin, M.E., 2009. A Common representative intermediates (CRI) mechanism for VOC degradation. Part 3: development of a secondary organic aerosol module. Atmos. Environ. 43, 1982–1990.

Utembe, S.R., Cooke, M.C., Archibald, A.T., Shallcross, D.E., Derwent, R.G., Jenkin, M.E., 2011. Simulating secondary organic aerosol in a 3-D Lagrangian chemistry transport model using the reduced common representative intermediates mechanism (CRI v2-R5). Atmos. Environ. 45, 1604–1614.

Valverde-Canossa, J., Wieprecht, W., Acher, K., Moortgat, G.K., 2005. H_2O_2 and organic peroxide measurements in an orographic cloud: the FEBUKO experiment. Atmos. Environ. 39, 4279–4290.

Wang, C.X., Chen, Z.M., 2006. Effect of CH_3OOH on the atmospheric concentration of OH radicals. Prog. Nat. Sci. 16, 1141–1149.

Wang, Y., Ridley, B., Fried, A., Cantrell, C., Davis, D., Chen, G., Snow, J., Heikes, B., Talbot, R., Dibb, J., Flocke, F., Weinheimer, A., Blake, N., Blake, D., Shetter, R., Lefer, B., Atlas, E., Coffey, M., Walega, J., Wert, B., 2003. Springtime photochemistry at northern mid and high latitudes. J. Geophys. Res. 108 (D4), 8358.

Wang, Y., Liu, S.C., Wine, P.H., Davis, D.D., Sandholm, S.T., Atlas, E.L., Avery, M.A., Blake, D.R., Blake, N.J., Brune, W.H., Heikes, B.G., Sachse, G.W., Shetter, R.E., Singh, H.B., Talbot, R.W., Tan, D., 2001. Factors controlling tropospheric O_3, OH, NO_x, and SO_2 over the tropical Pacific during PEM-tropics B. J. Geophys. Res. 106 (D23), 32733–32747.

Wang, Y., Jacob, D.J., 1998. Anthropogenic forcing on tropospheric ozone and OH since preindustrial times. J. Geophys. Res. 103, 31123–31135.

Watson, L.A., Shallcross, D.E., Utembe, S.R., Jenkin, M.E., 2008. A common representative intermediate (CRI) mechanism for VOC degradation. Part 2: gas phase mechanism reduction. Atmos. Environ. 42 (31), 7196–7204.

Weinstein-Lloyd, J.B., Lee, L.J., Daum, P.H., Kleinmann, L.I., Nunnermacker, L.J., Springston, S.R., 1998. Measurement of peroxides and related species during the 1995 summer intensive of the Southern oxidants study in Nashville, Tennessee. J. Geophys. Res. 103, 22361–22373.

Wild, O., Palmer, P.I., 2008. How sensitive is tropsopheric oxidation to anthropogenic amissions? Geophys. Res. Letts 35, L22802.

Zhang, X., Chen, Z.M., Wang, H.L., He, S.Z., Huang, D.M., 2009. An important pathway for ozonolysis of alpha-pinene and beta-pinene in aqueous phase and its implications. Atmos. Environ. 43, 4465–4471.

Zhang, X., He, S.Z., Chen, Z.M., Zhao, Y., Hua, W., 2012. Methyl hydroperoxide (CH_3OOH) in urban, suburban and rural atmosphere: ambient concentration, budget, and contribution to the atmospheric oxidizing capacity. Atmos. Chem. Phys. 12, 8951–8962.